

Inhibitory coupling specifically generates emergent gamma oscillations in diverse cell types

Vikaas S. Sohal* and John R. Huguenard†

Department of Neurology and Neurological Sciences, Stanford University School of Medicine, Stanford, CA 94305

Communicated by Edward G. Jones, University of California, Davis, CA, October 25, 2005 (received for review August 12, 2005)

Networks of inhibitory neurons regulate synchrony during many physiological and pathological oscillations. To explore how these effects depend on cellular, network, and synaptic factors, we developed and validated a semisynthetic inhibitory network that approximates simultaneous activity in multiple neurons by using consecutive responses from single cells. We recorded from three types of neurons, each of which forms interconnected networks *in vivo*, but has unique intrinsic properties. In all three cell types, fast inhibitory coupling generated emergent gamma oscillations. By contrast, inhibitory coupling desynchronized slower, spindle-frequency responses specifically in thalamic reticular neurons. The emergent gamma-frequency synchronization was also specific to tonic input and did not occur during responses to phasic inputs. These results illustrate how particular features of inhibitory networks (e.g., cell or input type) contribute to their synchronizing or desynchronizing functions. They also demonstrate phenomena (emergent gamma oscillations) that occur robustly in multiple cell types and may thus be a generic feature of inhibitory networks throughout the brain.

dynamic clamp | GABA_A receptor | neocortex | synchrony | thalamus

Oscillatory synchrony is central to many physiological and pathological neural processes and is typically controlled by networks of coupled inhibitory neurons. Several studies have elucidated mechanisms by which connections between fast-spiking (FS) cells contribute to gamma-frequency oscillations (30–100 Hz), which have proposed roles in perception and/or attention (1–3). Isolated networks of FS cells generate emergent gamma oscillations in response to tonic excitation in hippocampal slices (4). During these oscillations, inhibitory synapses between FS cells generate rhythmic fluctuations in inhibition, which both pace oscillations and generate synchrony (5–10). FS cells also fire phase-locked action potentials during gamma oscillations in entorhinal cortex slices (11). However, it is not known whether emergent gamma oscillations are a general feature of inhibitory networks throughout the brain or are specific to networks of hippocampal FS cells. In addition, excitatory neurons fire at particular phases of gamma oscillations and/or intrinsically oscillate at gamma frequencies and may contribute to gamma oscillations by rhythmically exciting interneurons (12–14). The role of inhibitory synapses between interneurons in synchronizing or desynchronizing gamma oscillations involving phasic excitatory feedback is unknown.

Whereas inhibitory synapses between FS cells are thought to synchronize gamma oscillations, inhibitory connections between thalamic reticular (RE) neurons suppress synchrony during spindle (6–14 Hz) oscillations, preventing the emergence of hypersynchronous epileptiform activity (15–18). During spindle oscillations, RE neurons fire Ca²⁺-dependent spikes, leading to synaptic inhibition of thalamic relay neurons, which then rebound burst and re-excite RE neurons (19). Thus, inhibitory neuron firing during spindles is driven by phasic excitatory feedback. It is not known whether the very different effects that intra-FS and intra-RE connections have on synchrony during emergent gamma oscillations and spindle oscillations, respectively, arise from differences in intrinsic cellular properties (e.g., Ca²⁺ currents in RE neurons), synaptic properties

(e.g., the slow kinetics of intra-RE inhibition), or other factors (e.g., the different frequencies of spindle and gamma oscillations or differences between phasic and tonic excitatory drive). Ideally, to answer these questions, one would induce spindle-frequency oscillations in FS cell networks (which normally generate gamma oscillations) and gamma-frequency oscillations in RE neuron networks (which normally participate in spindles), manipulate synaptic kinetics, and observe how inhibitory coupling affects synchrony in each case.

Here, we describe a semisynthetic network (*cf.* ref. 20) composed of different classes of inhibitory neurons and use it to address the questions raised above. First, we validate our semisynthetic approach. Second, we study whether networks composed of various cell types generate emergent gamma oscillations in response to tonic excitation. Third, we show how inhibitory coupling affects synchrony during oscillations driven by phasic excitation. Finally, we use simulations to verify that our results do not depend on the details of our semisynthetic approach.

Methods

Slice Preparation. Experiments were performed in accordance with procedures established by the Administrative Panel on Laboratory Animal Care at Stanford University. Briefly, postnatal day 13 (P13) through P20 Sprague–Dawley rats were anesthetized with pentobarbital. Using a vibratome, we cut 200- μ m horizontal slices (thalamic experiments) or 250- μ m coronal slices (neocortical experiments) in a chilled, oxygenated slicing solution consisting of 234 mM sucrose, 11 mM glucose, 24 mM NaHCO₃, 2.5 mM KCl, 1.25 mM NaH₂PO₄, 10 mM MgSO₄, and 0.5 mM CaCl. Slices were incubated in 32°C oxygenated artificial cerebrospinal fluid (ACSF) for at least 1 h before recording. ACSF consisted of 126 mM NaCl, 26 mM NaHCO₃, 2.5 mM KCl, 1.25 mM NaH₂PO₄, 1 mM MgCl₂, 2 mM CaCl, and 10 mM glucose. In the recording chamber, slices were maintained at 32–33°C and superfused with ACSF.

Intracellular Recording. Whole-cell patch recordings were made from visually identified neurons of the thalamic RE nucleus or layer V neocortical interneurons by using IR video microscopy with Nomarski optics and a Multiclamp 700A amplifier (Axon Instruments, Union City, CA). Patch electrodes (tip resistance = 3–4 M Ω) were filled with 131 mM K-gluconate, 8 mM KCl, 2 mM NaCl, 10 mM Hepes, 3 mM EGTA, 4 mM MgATP, and 0.3 mM NaGTP. pH was adjusted to 7.3 by using KOH. The liquid junction potential was estimated at 14 mV, and the membrane potential was adjusted accordingly. During all recordings, ionotropic glutamate and GABA receptors were blocked by bath-applied 6,7-dinitroquinoxaline-

Conflict of interest statement: No conflicts declared.

Abbreviations: FS, fast-spiking; RE, reticular; EPSC, excitatory postsynaptic current; RIN, recursive inhibitory network; IPSC, inhibitory postsynaptic current.

*Present address: Department of Psychiatry, Stanford University School of Medicine, Stanford, CA 94305.

†To whom correspondence should be addressed. E-mail: john.huguenard@stanford.edu.

© 2005 by The National Academy of Sciences of the USA

line-2,3-dione (20 μM), 2-amino-5-phosphopentanoic acid (50 μM), and picrotoxin (50 μM).

Current clamp firing behavior and cell morphology were used to differentiate neocortical interneurons from pyramidal cells. Current clamp firing behavior also classified interneurons as FS ($n = 6$ cells) or non-FS ($n = 6$ cells). For FS and non-FS cells, the ratio between the fourth and last interspike intervals was 1.03 ± 0.02 and 0.78 ± 0.05 , respectively (during 200-ms injection of 360 pA). Action potential half-widths were 0.23 ± 0.02 and 0.33 ± 0.04 ms for FS and non-FS cells, respectively.

Dynamic Clamp. Dynamic clamp was implemented by using custom-written software running under the Real Time Application Interface for Linux (www.aero.polimi.it/~rtai). Synaptic currents were modeled by $I_{\text{syn}} = g_{\text{syn}}(E_{\text{syn}} - V_m)$, where g_{syn} (synaptic conductance) and V_m (membrane potential) were updated at 5–10 kHz. E_{syn} represents reversal potential. Whenever a virtual synaptic event occurred, g_{syn} was incremented by a fixed amount, representing the amplitude of an individual synaptic event, and thereafter decayed exponentially with a time constant, τ_{decay} . For excitatory synapses, $E_{\text{syn}} = 0$ mV and $\tau_{\text{decay}} = 2$ ms. Inhibitory synapses had variable decay kinetics, but E_{syn} was always -75 mV. Bridge balance was adjusted throughout experiments, insuring accurate V_m measurements. The series resistance was usually 10–20 M Ω , and experiments were discontinued if the bridge balance exceeded 30 M Ω . A two-electrode dynamic clamp has been used (21), but a recent study found nearly identical results using two-electrode and one-electrode approaches (22). Dynamic clamp approximates excitatory postsynaptic currents (EPSCs) by using somatic current injections. Although many excitatory inputs are located beyond the soma, somatic current injection has been used in many studies of synchrony in response to excitatory input (20, 23). During experiments, each sweep was 1 s long, and there were 2 s between sweeps.

Recursive Inhibitory Network (RIN) Parameters. For a recording from one neuron, all inhibitory postsynaptic currents (IPSCs) had the same amplitude. The peak amplitude was either 12 or 16 nS when τ_{decay} was 4 ms and was scaled down by a factor of 8 when τ_{decay} was 32 ms. We used inhibitory conductances in the 12- to 16-nS range because at this level introducing IPSCs reduced the number of spikes by $\approx 50\%$. Inhibitory connections between FS cells *in vitro* have amplitudes ≈ 5 nS (8). Our connections are slightly stronger, because there are only five inhibitory inputs to each virtual neuron in a RIN, whereas neurons *in vitro* and *in vivo* probably receive larger numbers of inhibitory inputs.

The amount of tonic current and EPSC amplitude was adjusted on a neuron-by-neuron basis to produce firing rates ≈ 50 –60 Hz in response to the input stimuli. While recording from a given neuron, as we changed the type of input, we fixed the EPSC amplitude. For RE, FS, and non-FS cells, ranges of EPSC amplitudes were 9–12, 5–6, and 4–15 nS, respectively.

All data in the text and figures are reported as mean \pm SEM.

Analysis. The peri-stimulus time histogram (PSTH) was computed for each neuron by using 2-ms-wide bins. To calculate cross-correlation for an experiment, we first subtracted the mean firing rate (in spikes per bin) from the PSTH, then used this corrected PSTH to compute the cross-correlation.

To compute the spectral coherence, we first calculated the Fourier transform of each virtual neuron's spike rate as a function of time, using 2-ms-wide bins and windows that were 200 ms wide and spaced 50 ms apart. Let $F_i(\omega, t)$ denote the Fourier transform of virtual neuron i 's spike train as a function of time and frequency. Then, we defined $C_{ij}(\omega)$, the coherence between virtual neurons i and j as the real part of the zero time lag cross-correlation of $F_i(\omega, t)$ and $F_j(\omega, t)$, i.e.,

$$C_{ij}(\omega) = \frac{\sum_t F_i(\omega, t) \cdot \overline{F_j(\omega, t)}}{\sqrt{\sum_t F_i(\omega, t) \cdot \overline{F_i(\omega, t)} \sum_t F_j(\omega, t) \cdot \overline{F_j(\omega, t)}}}$$

[$\overline{F_j(\omega, t)}$ is the complex conjugate of $F_j(\omega, t)$]. Thus, when the Fourier coefficients are out of phase, their contribution to the coherence is zero, and when they are in phase, their contribution is related to the product of their amplitudes.

Computational Modeling. All simulations used NEURON (24) at a temperature of 32°C and with a time step of 0.1 ms. Data have been averaged over multiple simulations, each with different values for random parameters, e.g., EPSC times, the pattern of connectivity, V_m , etc. Unless otherwise specified, all of our simulations contained 10 FS cells, each of which received GABA_A receptor-mediated connections from five other FS cells. For “directional coupling,” the FS cells were arranged in a ring and each FS cell received connections from its five neighbors in one direction along the ring, whereas for “random coupling,” each FS cell received connections from five other randomly chosen FS cells (no FS cell made more than one connection with another FS cell, and there were no autapses). Detailed parameters are found in *Supporting Text*, which is published as supporting information on the PNAS web site.

Results

Constructing RINs. To construct semisynthetic inhibitory networks, we blocked endogenous synaptic transmission and used a dynamic clamp (25) to inject a neuron with realistic trains of EPSCs. Then we implemented IPSCs by using action potential times on one sweep to trigger IPSCs on later sweeps. As we will now show, when this approach is implemented appropriately, responses of a single neuron on consecutive sweeps closely approximate activity in a network composed of multiple neurons with similar intrinsic properties.

A “stimulus” is the train of EPSCs injected on a particular sweep. During each experiment, 10 prespecified stimuli, S_1, S_2, \dots, S_{10} , were repeatedly presented in sequence, e.g., stimulus S_2 was presented on sweeps 2, 12, 22, etc. (the way we constructed stimuli is described in detail below). Whereas excitatory stimuli were prespecified and repeatedly presented in sequence, the times of IPSCs on each sweep were determined by the times of spikes from the previous five sweeps (representing five upstream neurons). The times of IPSCs on sweep 6 were based on the times of spikes on sweeps 1–5, so that neuron 6 was postsynaptic to neurons 1–5. Fig. 1A shows this setup.

Suppose that eventually the responses to the stimuli converge to a fixed set of 10 responses, i.e., the response on sweep 41 is the same as that on sweeps 51, 61, etc. Then let the response on sweep 41 represent the response of “virtual neuron 1.” Define responses of virtual neurons 2–10 similarly. This only makes sense if the responses converge, and we will show that this convergence occurs. Because spikes during each sweep trigger IPSCs during the next five sweeps, each virtual neuron is presynaptic to the next five virtual neurons. In this way, the 10 virtual neurons constitute a RIN, which corresponds to an interconnected ring of 10 neurons, in which each neuron inhibits its five neighbors in one direction along the ring, as shown in Fig. 1B. Note that if the convergence is exact, then the set of responses to the 10 stimuli exactly replicates activity in an actual ring of 10 neurons interconnected by this pattern. If the convergence is approximate, then the responses to the 10 stimuli approximate responses in the interconnected ring (later we will show that this approximation is highly precise).

RINs are similar to iteratively constructed networks (ICNs) (20), but unlike ICNs, which exactly reproduce activity in feed-forward networks, RINs approximate activity in networks with feedback connections. Note that while the connections in our RINs were “directional” in the sense that each neuron inhibited five neighbors in one direction along the ring, each neuron also received feedback

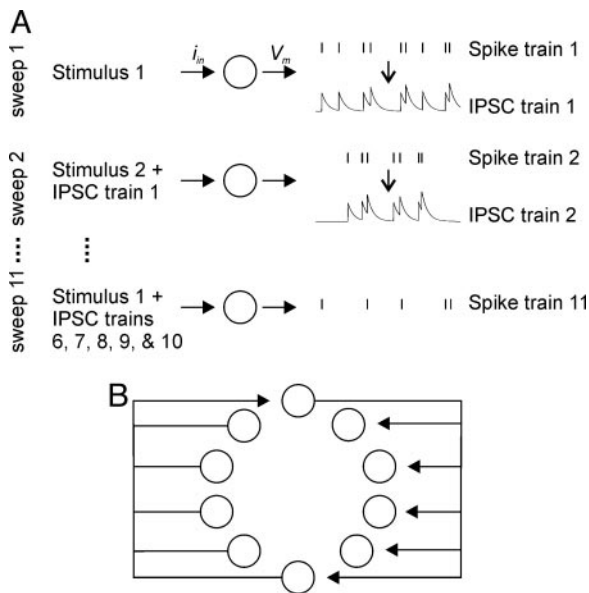


Fig. 1. Experimental design. (A) We presented excitatory stimulus i on sweeps $i, i + 10$, etc. Responses to repeated presentations of the same stimulus represent successive approximations for the response of a virtual neuron within the semisynthetic network. IPSC times on each sweep were determined by the times of spikes on the preceding five sweeps. (B) Ten consecutive responses during a RIN experiment should approximate the simultaneous responses of 10 “virtual neurons” arranged in a ring, in which each virtual neuron inhibits five neighbors in one direction and receives inhibition from five neighbors in the opposite direction. Connections to/from one virtual neuron are shown.

inhibition from one of these five neighboring neurons. Later we will demonstrate that random feedback connections produce the same results as this semidirectional coupling.

Simulated RINs Accurately Approximate Activity in Simulated Networks. We next sought to verify that RINs accurately reproduce activity in actual networks. As explained above, convergence in-sures such fidelity. In every RIN we studied, regardless of cell type or stimulus pattern, repeated presentations of the 10 excitatory stimuli along with synthetic synaptic inhibition elicited virtual neuron responses that converged to a stable set of 10 responses. Fig. 2A shows successive responses from one virtual neuron in one RIN, and Fig. 2B plots the average rate of convergence based on 73 experiments in recordings from 21 neurons. As Fig. 2 shows, the response to the fifth presentation of a stimulus was very similar to the response to the fourth presentation, demonstrating that activity converged after four or five presentations, i.e., the response on sweep $i + 30$ was very similar to the responses on sweeps $i + 40, i + 50$, etc., for $i = 1, 2, \dots, 10$.

For additional confirmation, we used computational modeling. We simulated activity in a network of 10 neurons (“simulated network”) and in the corresponding RIN (“simulated RIN”). A simulated RIN was a simulation of a single-model neuron, which we repeatedly stimulated by using the procedure described above, i.e., a simulation of the experiment we did to construct a RIN from an actual neuron. In a network, activity of all 10 neurons evolved simultaneously, in parallel, whereas in a RIN experiment or in a simulated RIN, the activity of each virtual neuron was computed serially. The simulated network and simulated RIN used the same excitatory stimuli, pattern of connectivity, synaptic and cellular parameters, etc. By comparing spike times, we found that the activity of each virtual neuron in the simulated RIN converged to that of its counterpart in the simulated network.

We systematically matched spikes from simulated networks with

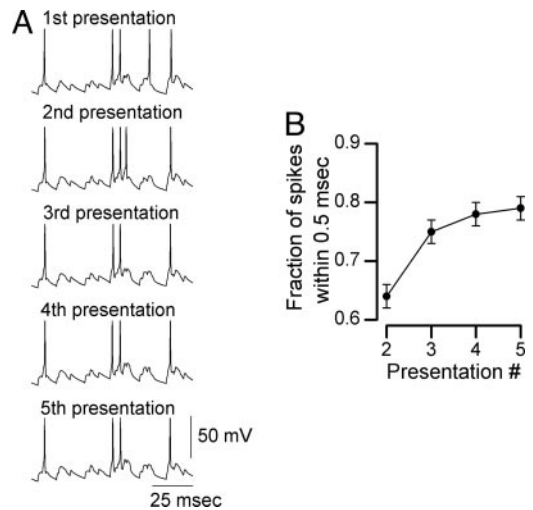


Fig. 2. Activity in RINs converges. To construct a RIN, we repeatedly injected a neuron with the same sequence of 10 stimuli. (A) Responses to the first, second, etc. presentations of the same stimulus. (B) The fraction of spikes that occur within 0.5 ms of a spike during the previous presentation of the same stimulus, as a function of presentation number. By the fourth or fifth presentation, $\approx 80\%$ of the spikes occur at stereotyped times ($n = 73$ experiments from 21 cells). (Error bars, \pm SEM.)

those from the corresponding simulated RINs (and vice versa) and computed time differences for pairs of matching spikes. Simulations used various types of excitatory stimuli, described below in more detail. During responses to noisy tonic excitation, 87% of spikes matched with a time difference of <1 ms, and during responses to phasic excitation of varying frequencies, $>99\%$ of spikes matched with a time difference of <0.5 ms ($n = 4$ simulations for each case). Thus, simulated RINs accurately reproduce activity in the corresponding simulated networks.

Emergent Gamma Oscillations Are a General Feature of Inhibitory Networks. Having validated the RIN approach by showing that RIN activity converges *in vitro*, and that RINs accurately model simulated inhibitory networks, we constructed RINs by making whole-cell dynamic clamp recordings from RE neurons ($n = 9$) and two major classes of neocortical interneurons (26, 27), FS ($n = 6$) and non-FS cells ($n = 6$). (Note, unless otherwise specified, RIN refers to an experiment using the RIN approach with biological neurons. We used the terms simulated RIN or simulations to refer to results from computational modeling.) In our first set of experiments, we studied whether these three types of inhibitory neurons, which have very different intrinsic properties, could generate emergent gamma oscillations, which have previously only been described for networks of FS cells. We found that regardless of cell type inhibitory networks invariably generated synchronized gamma oscillations in response to tonic excitation. Fig. 3A shows five consecutive responses of an example RE cell, representing five virtual neurons within a RIN, in the presence and absence of inhibitory coupling. In this experiment, each virtual neuron received “noisy tonic” input, i.e., a variable amount of tonic current, representing heterogeneity, and a different Poisson train of EPSCs, representing noise (the amplitudes of the tonic current were chosen from a uniform distribution with a width of 40 pA, and the center of this distribution was chosen to produce firing rates ≈ 100 Hz in the absence of inhibition). Firing was uncorrelated in the absence of inhibition, but when inhibitory coupling was present, firing was rhythmic and synchronized (e.g., Fig. 3A).

We quantified the effect of inhibitory coupling on network activity in two ways. First, we computed the spectral coherence (see *Methods*) between spike trains from different virtual neurons in the

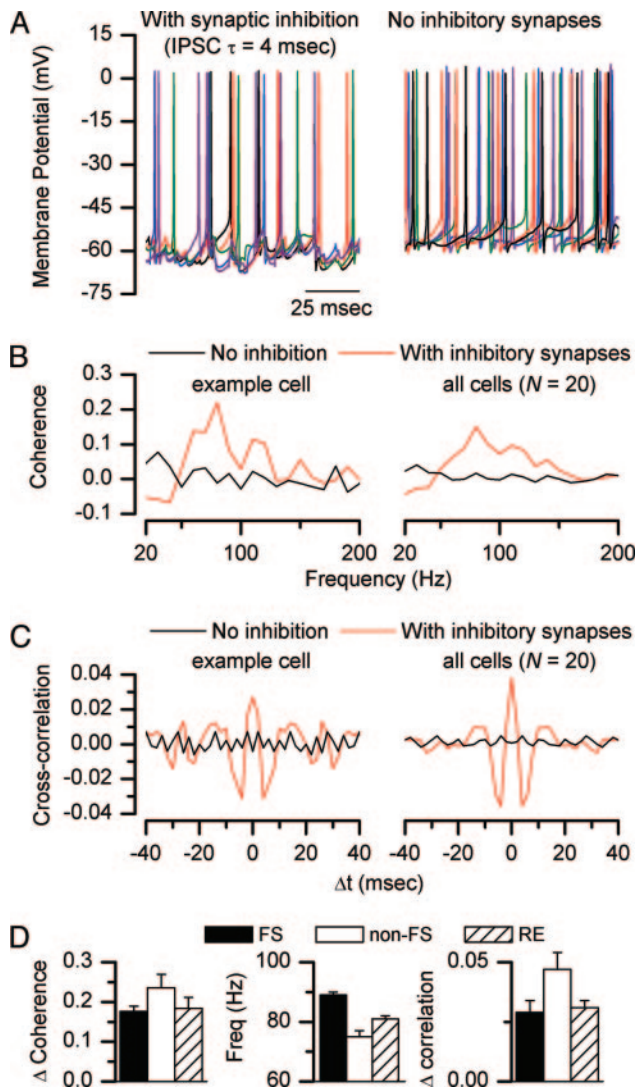


Fig. 3. Fast inhibition generates emergent gamma oscillations in all cell types. (A) Five consecutive responses of an RE cell to tonic current (plus noise), representing the responses of five different virtual neurons, when fast inhibitory coupling is present (Left) or absent (Right). (B) (Left) Coherence in the gamma frequency range is higher when inhibitory coupling is present (red line) than when it is absent (black line). The coherence function was calculated from responses to tonic input of the 10 virtual neurons represented by the RE cell depicted in A. (Right) Coherence function averaged over responses from all neurons to tonic input ($n = 20$ cells). (C) (Left) The cross-correlation is flat in the absence of inhibition (black line), but after adding inhibitory coupling (red line), a prominent central peak, side peaks and troughs appear. The cross-correlogram was calculated by using the responses to tonic input of the 10 virtual neurons represented by the RE cell depicted in A. (Right) Cross-correlogram averaged over responses of all neurons to tonic input ($n = 20$ cells). (D) (Left) Average increase in peak gamma coherence (PGC) induced by fast inhibitory coupling during responses to tonic input, as a function of cell type. (Center) Average frequency at which PGC occurred as a function of cell type. (Right) Average increase in the peak cross-correlation induced by fast inhibitory coupling during responses to tonic input, as a function of cell type. (Error bars, \pm SEM.)

RIN. We first calculated the coherence based on responses to stimuli alone (no IPSCs). Then we introduced IPSCs as described above, and after network activity had converged (e.g., after 40 sweeps), we again calculated the coherence. Fig. 3B Left shows the coherence spectrum for the RIN depicted in Fig. 3A, when inhibition is present (red line) or absent (black line). In this case, adding inhibitory synapses increased coherence in the gamma band (30–

100 Hz), indicating synchronized gamma-frequency activity. Inhibitory coupling produced a similar effect in the population average coherence spectrum (Fig. 3B Right), which was computed from responses of all three cell types to noisy tonic input ($n = 20$ cells). For each experiment, we found that inhibitory coupling significantly increased peak gamma band coherence (Fig. 3D Left) in RINs constructed from either FS, non-FS, or RE cells (each case, $n = 6$ –8 cells, $P < 0.001$). The amount of gamma band coherence did not differ between cell types ($P = 0.29$, one-way ANOVA), but cell type did have a significant effect on the frequency at which peak gamma band coherence occurred: 89 ± 1 Hz in FS cells, 75 ± 2 Hz in non-FS cells, and 81 ± 1 Hz in RE cells ($P < 0.05$, one-way ANOVA; Fig. 3D Center). There was no correlation between frequency and either passive membrane properties or the amplitude of injected current ($P = 0.48$, multiple linear regression), suggesting that active, not passive, conductances determine the oscillation frequency.

We also measured the effect of inhibitory coupling on network activity by using cross-correlation. We computed cross-correlations after subtracting the mean firing rate from the peri-stimulus time histogram, so as to measure only correlations between phasic changes in the level of activity, not correlations between the mean firing rates of two virtual neurons. For each experiment, we averaged cross-correlograms from all pairs of virtual neurons. Fig. 3C Left shows the cross-correlation averaged for the RE cell depicted in Fig. 3A and B. As expected, without inhibitory coupling (Fig. 3C Left, black line), there were no correlations between different virtual neurons. However, when inhibitory coupling was present (Fig. 3C Left, red line), the cross-correlation had a central peak surrounded by deep troughs, indicating emergent synchrony, and secondary peaks at $\Delta t = 14$ and 26 ms, indicating rhythmicity. Fig. 3C Right shows a similar effect in the population average cross-correlation, computed from responses of all three cell types to noisy tonic input ($n = 20$ cells). Fig. 3D Right shows that adding inhibitory coupling significantly increased the peak cross-correlation, a measure of synchrony, in RINs constructed from FS, non-FS, or RE cells (each case, $n = 6$ –8 cells, $P < 0.001$). The relatively low amplitude of the cross-correlation function results from the small bin width (2 ms) used to compute cross-correlations, and the fact that we subtracted the mean firing rate, eliminating correlations between mean firing rates. The cross-correlograms shown here are highly damped, because of cycle-to-cycle variability in the frequency and phase of oscillations. This damping is similar to that observed during gamma oscillations *in vivo* (28, 29). [Note: covariation in neural excitation, in addition to spike-timing synchrony, can produce peaks in the cross-correlation (30). However, covariation in excitability would also be expected to produce peaks in the cross-correlogram in the absence of inhibition, which were not observed.]

Slow Inhibition Fails to Generate Synchronized Oscillations. Because fast inhibitory coupling produced emergent gamma oscillations in RINs constructed from disparate cell types, we studied whether slower inhibition ($\tau_{decay} = 32$ ms), characteristic of inhibitory synapses between RE cells (16), produced similar effects. During our experiments, the amplitude of the inhibitory conductance associated with slow IPSCs was always one-eighth that of fast IPSCs, so that the time integral of each inhibitory postsynaptic conductance was constant, regardless of τ_{decay} . (This was necessary because slowing inhibitory events without decreasing their amplitude profoundly suppressed firing rates. We found that after normalizing inhibitory conductances, fast and slow inhibition yielded similar firing rates.) We found that slow inhibitory coupling failed to generate gamma frequency synchrony, as measured by cross-correlation and peak gamma coherence (*cf.* ref. 8).

Effects of Inhibition on Responses to Rhythmic Input. Having studied emergent gamma oscillations, we shifted attention to oscillations

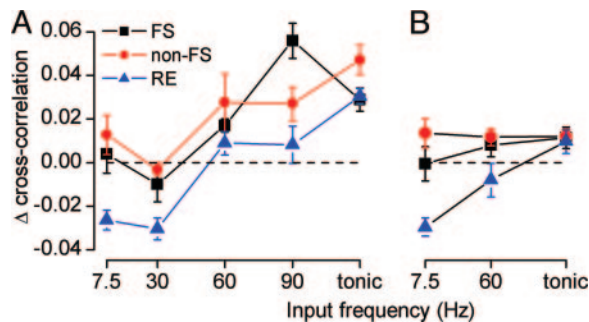


Fig. 4. Effects of inhibitory coupling on synchrony. (A) Effects of fast inhibitory coupling on synchrony (measured by the peak cross-correlation) as a function of input frequency and cell type ($n = 6$ FS cells, $n = 4$ – 6 non-FS cells, and $n = 4$ – 9 RE cells, for each frequency). (B) Effects of slow, weak inhibitory coupling on synchrony (measured by the peak cross-correlation) as a function of input frequency and cell type ($n = 4$ – 5 FS cells, $n = 3$ non-FS cells, and $n = 4$ – 5 RE cells, for each frequency). (Error bars, \pm SEM.)

driven by rhythmic excitation. To model these oscillations, we used stimuli consisting of rhythmically occurring EPSCs, generated with Poisson statistics, where the EPSC rate was the sum of a sinusoidal, time-varying component (representing rhythmic excitation) and a constant component (representing noise). For different virtual neurons within each RIN, rate functions had identical amplitude and phase, but the times of individual EPSCs were different. To study oscillations of different frequencies, we simply changed the frequency of the sinusoidal component of the EPSC rate function. As described above, IPSCs decayed with either fast or slow kinetics, and the amplitude of individual slow IPSCs was normalized.

Fig. 4 summarizes how inhibition affects synchrony as a function of input type (e.g., tonic vs. phasic, input frequency), cell type, and synaptic kinetics. Our major finding was that both fast and slow inhibitory coupling selectively desynchronized RE cell responses to spindle-frequency (7.5 Hz) input (fast inhibition: $P < 0.001$, $n = 8$ cells; slow inhibition, $P < 0.05$, $n = 4$ cells). Both fast and slow inhibition were more desynchronizing in RE cells than in FS (fast inhibition, $P < 0.05$, $n = 6$ cells; slow inhibition, $P < 0.05$, $n = 3$ cells) or non-FS cells (fast inhibition, $P < 0.001$, $n = 6$ cells; slow inhibition, $P < 0.01$, $n = 3$ cells).

Inhibitory Coupling Desynchronizes Spindle-Frequency Activity in RE Cells.

The different effects of inhibition on spindle-frequency activity in RE cells and other cell types can be understood as follows. During troughs of the oscillation, RE cells responded weakly, whereas other cell types fired significantly more (e.g., trough firing rate = 13 ± 1 Hz and 49 ± 11 Hz in RE and FS cells, respectively; $P < 0.05$). As a result, in RE cells, inhibition had little effect on trough firing, which was low even in the absence of inhibition (e.g., slow inhibition only reduced trough firing from 13 ± 1 to 7 ± 1 Hz), whereas in other cell types, inhibition markedly reduced trough firing (e.g., in FS cells, slow inhibition reduced trough firing from 49 ± 11 to 11 ± 1 Hz). Thus, the main effect of inhibitory coupling in RE cells was to suppress peak firing, thereby suppressing synchrony. By contrast, in other cell types, inhibition suppressed both peak and trough firing, producing no net change in synchrony.

Effects of Inhibition on Synchrony and Rhythmicity Are Robust to Changes in Network Architecture.

To complement results obtained with the RIN approach with actual neurons, we simulated networks of interconnected inhibitory neurons and varied network architecture, intrinsic cellular properties, synaptic properties, etc. Model neurons consisted of single compartments with Hodgkin–Huxley-type Na^+ and K^+ currents. In every case described below, we did four simulations for each condition.

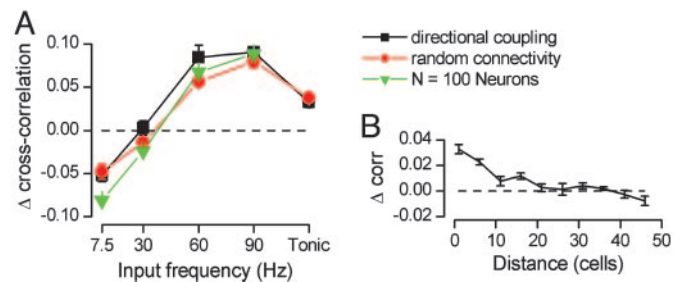


Fig. 5. Simulations show that experimental results obtained with RINs are valid under more general conditions. (A) Inhibitory coupling produces similar effects on synchrony (measured by the peak cross-correlation) in simulated inhibitory networks with directional coupling (black line), random connectivity (red line), and in a large network of 100 model neurons (green line). (B) Inhibitory coupling generates emergent distance-dependent synchronization during responses to tonic input in a large network of 100 neurons, with local connectivity.

First, we simulated different patterns of connectivity. We simulated networks with directional coupling, corresponding to the situation in RIN experiments, in which each neuron synapses onto five neighbors in one direction along the ring. Using fast synapses ($\tau_{\text{decay}} = 4$ ms, $g_{\text{rel}} = 1.0$), we compared the effect of directional inhibitory coupling with that of random inhibitory coupling and found precisely the same effects on synchrony in both cases (Fig. 5A). We also simulated large networks ($n = 100$ model neurons), in which each neuron inhibited 10 neighboring neurons in each direction. During responses to rhythmic input, we again found the same effects (Fig. 5A), and during responses to noisy tonic excitation we observed emergent local (although not networkwide) synchronization (Fig. 5B).

Finally, we studied the effects of heterogeneity. The coefficient of variation (CV, the ratio of the standard deviation to the mean) is ≈ 0.2 for FS-FS IPSC amplitude (8). In our recordings from neocortical FS cells ($n = 6$ cells), the resting membrane potential (V_m) and input conductance (g_{leak}) were -72 ± 7 mV and 8.5 ± 1.2 nS (mean \pm SD), respectively. Therefore, we simulated responses to noisy tonic inputs in RINs and networks for which the CV for IPSC amplitude, V_m , and g_{leak} were $0.2\times$, $0.1\times$, and $0.14\times$, respectively (the heterogeneity index, x , measures heterogeneity). We simulated values of x between 0 and 1.33 and found that both convergence and emergent gamma oscillations were robust to heterogeneity in this range (see Fig. 6, which is published as supporting information on the PNAS web site). The results of these simulations suggest that our findings are not artifacts of (i) the connectivity scheme we have chosen, (ii) the fact that each RIN is based on a recording from a single neuron, or (iii) the size of the RIN used in experiments (10 virtual neurons).

To explore the possibility that the failure of “slow” inhibitory to generate emergent gamma rhythmicity resulted from the normalized amplitude, rather than the kinetics of slow inhibition, we also simulated networks with slow, but strong, inhibitory connections. In such networks, the cross-correlogram lacked many characteristic features of gamma-frequency synchrony, e.g., there was a central peak, but it was very wide (≈ 10 ms), there were no troughs abutting the central peak, and side peaks indicative of rhythmicity were absent. (see Fig. 7, which is published as supporting information on the PNAS web site).

Effect of Gap Junctions. Gap junctions are often present between inhibitory neurons of the same class (31–33) and make important contributions to rhythmic synchrony (34–38). Because our RINs did not include gap junctions, we wanted to confirm that adding gap junctions would not alter our major results. Indeed, in simulations, we found that adding gap junctions induced synchrony, but that

